Nano Energy 103 (2022) 107829

Contents lists available at ScienceDirect

Nano Energy

journal homepage: www.elsevier.com/locate/nanoen

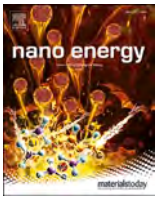

Long-life silicon anodes by conformal molecular-deposited polyurea interface for lithium ion batteries

Tiansheng Mu [a,b], Yipeng Sun [b], Changhong Wang [b], Yang Zhao [b], Kieran Doyle-Davis [b], Jianneng Liang [b], Xulei Sui [b], Ruying Li [b], Chunyu Du [a], Pengjian Zuo [a,*], Geping Yin [a,*], Xueliang Sun [b,*]

[a] MIIT Key Laboratory of Critical Materials Technology for New Energy Conversion and Storage, School of Chemistry and Chemical Engineering, Harbin Institute of Technology, Harbin 150001, China
[b] Department of Mechanical and Materials Engineering, University of Western Ontario, London, Ontario N6A 5B9, Canada

ARTICLE INFO

Keywords:
Silicon anodes
Transport kinetics
Polyurea interface
Lithium ion batteries

ABSTRACT

Establishing a stable electrode-electrolyte interface (SEI) is extremely critical to achieving a reversible silicon anode for lithium ion batteries. Herein, a conformal polyurea layer with hydrogen bonds and polar functional groups is firstly controllably constructed on the silicon electrode as an artificial SEI via molecular layer deposition. The optimized polyurea coating of ~3 nm greatly promotes the electrochemical lithium storage performance of silicon anodes, including highly reversible cycling stability (1010 mA h g^{-1} after 1000 cycles) and rate capability (1820 mA h g^{-1} at 2 A g^{-1}, 1420 mA h g^{-1} at 5 A g^{-1}). Analyses show that this polyurea layer can greatly promote lithium ions diffusion kinetic in the silicon electrodes and induce a stable, thin, and LiF-rich SEI with good mechanical stability. Moreover, this polyurea coating shows a significant improvement for larger-size silicon particles (even >150 nm) and superior compatibility with ether-based electrolytes. Notably, the full cells paired with $LiFePO_4$ cathode exhibit impressive cycling stability with a high energy density of 453 Wh kg^{-1}. This work provides constructive guidance for constructing a stable artificial SEI for silicon anodes.

1. Introduction

With the rise of green energy, the limited energy density of current state-of-the-art lithium-ion batteries (LIBs) has caused widespread concern [1]. Developing electrode materials with a high specific capacity is an effective way to increase the energy density of LIBs [2]. In this regard, silicon anode based on alloying mechanism is one of the best candidates for replacing the commercial graphite anode due to the outstanding capacity advantage (4200 mAh g^{-1}), environmental friendliness, and cost-effectiveness. However, the commercial application of silicon anode is hindered by serious volume swelling/shrinkage (>300%) and continuous interfacial side reaction, which lead to low Coulombic efficiencies, unsatisfactory cycling stability, and poor rate capability [3]. Mitigating volume change and stabilizing the silicon/electrolyte interface are key to realizing stable silicon anodes.

Typically, the solid electrolyte interphase (SEI), as a passivation layer, plays an important role for achieving a stable anode-electrolyte interface [4,5]. Unfortunately, the SEI of silicon anode in commercial carbonate electrolyte is mechanically fragile and insufficient to withstand the large volume fluctuation during cycling [6,7]. Generally, one effective approach to improve the SEIs stability is to use electrolyte additives. Fluoroethylene carbonate (FEC) vinylene carbonate (VC) additives have been proven to improve interface stability of silicon anodes, while some multifunctional additives are constantly being explored [6–9]. However, the continuous consumption of electrolyte additives during cycling prohibits the long-term viability of the silicon anode, and the slow dynamics of the additive-induced interface also severely limits the rate capability. Another effective approach capable of enhancing the SEI stability is to establish an artificial SEI [10]. Some artificial inorganic coatings have been extensively studied such as Al_2O_3, TiO_2 [11–15]. Although the interface chemical/electrochemical stability has been improved, the coating fracture caused by mechanical fragility is still a potential risk to the long-term service life of silicon anodes.

Compared to an inorganic coating, a polymer coating displays great advantages as an artificial layer due to good flexibility, which can withstand huge mechanical stress and prevent the plastic expansion of

* Corresponding authors.
E-mail addresses: zuopj@hit.edu.cn (P. Zuo), yingeping@hit.edu.cn (G. Yin), xsun9@uwo.ca (X. Sun).

https://doi.org/10.1016/j.nanoen.2022.107829
Received 3 July 2022; Received in revised form 12 August 2022; Accepted 18 September 2022
Available online 20 September 2022
2211-2855/© 2022 Published by Elsevier Ltd.

silicon anode [16,17]. Several conductive or non-conductive polymers have been employed to passivate the silicon-electrolyte interface such as polybithiophene, polyparaphenylene, and polyaniline [18–23]. Meanwhile, some polymer layer can promote the wettability of the electrolyte and silicon particles [21]. However, the structure and composition homogeneity of polymer layers based on wet chemical methods still faces challenges, which poses obstacles to uniform lithium ion transport kinetics at the silicon particle and electrode scale [24]. Currently, Shen's group proposed a silicon-containing polymer coated silicon electrode via initiated chemical vapor deposition. Although an improved electrochemical performance was obtained, the cycling lifespan was still seriously limited (100 cycles) [22]. Although some MLD polymer interfaces have been constructed on silicon anodes, these previous studies tend to focus only on the mechanical properties of the polymer layers, while ignoring the effect of interface chemistry on the electrochemical performance [25,26]. Furthermore, the chemistry/electrochemical stabilization mechanism of the polymer-silicon interface still remain unclear, which limits the design and development of artificial polymer SEI for silicon anodes. Therefore, establishing a stable SEI capable of long-cycling lifespan still faces huge challenges.

Herein, a conformal polyurea layer with hydrogen bonds and polar functional groups was controllably deposited on the silicon electrode as a robust artificial SEI via molecular layer deposition (MLD). The cycling stability of the silicon anode strongly depends on the polyurea coating thickness, and the optimal coating thickness was confirmed to be ~3 nm. And this polyurea coating can greatly accelerate the lithium ions diffusion kinetics and improve the cycling stability and rate capability of silicon anode, even for larger silicon particles (>150 nm). The key to the interface stabilization is the formation of a robust, thin, and LiF-rich SEI with good mechanical stability, which buffers the volume change and ensures the structural integrity of silicon electrodes. Simultaneously, the polyurea coating exhibits good compatibility with the ether-based electrolytes. Besides, the energy density of full battery paired with $LiFePO_4$ cathode can reach 453 Wh kg^{-1}. Importantly, this work provides new opinions on constructing an effective artificial SEI on the silicon anodes.

2. Experimental section

2.1. The polyurea coated silicon electrode

The silicon electrodes include silicon nanoparticles (80 wt%), Super P (10 wt%), and sodium carboxymethyl cellulose (10 wt%). The silicon electrodes were punched with a diameter of 10 mm. The active mass loading is approximately 1 mg cm^{-2}. The effect of silicon particle size was also explored, with sizes of ~150 nm, ~230 nm. The corresponding mass loadings of active materials are approximately 1.0 mg cm^{-2} for 150 nm silicon particles electrode and 2.0 mg cm^{-2} for 230 nm silicon particles electrode, respectively. The polyurea coating was directly deposited on the silicon electrodes. Specifically, the coating procedure was conducted by an Arradiance GEMstar-8 ALD machine. Ethylenediamine (ED) and 1,4-phenylene diisocyanate (PDIC) were used as precursors and purchased from Sigma-Aldrich. The precursors are stored in steel containers to isolate from air and moisture. To obtain enough vapor pressure, PDIC was pre-heated to 90 °C, while ED was kept at room temperature. During coating, the MLD chamber was heated to 65 °C. A full cycle of MLD polyurea (PU) was described as follows: ED pulse/purge/PDIC pulse/purge with durations of 0.2/30/1/30 s. different polyurea coated silicon electrodes were prepared by controlling the number of MLD cycles.

2.2. Characterizations

Powder X-ray diffraction (XRD) patterns were analyzed on a Bruker D8 X-ray diffractometer with Cu Kα (λ = 1.5406 Å) radiation. The morphology of the electrode was characterized by a Hitachi S-4800 field emission scanning electron microscope, a Hitachi 3400 N environmental scanning electron microscope, and a high-resolution transmission electron microscopy (JEOL 2010 FEG). X-ray photoelectron spectroscopy (XPS) was measured with a monochromatic Al Kα source (1486.6 eV) in a Kratos AXIS Nova Spectrometer. The TOF-SIMS tests were conducted using TOF-SIMS IV (ION-TOF GmbH, Germany) with a 25 keV bismuth liquid metal ion source with a base pressure at ~10^{-8} mbar in the analysis chamber. Negative secondary ions were induced by the primary ion beam bombardment on the surface of cycled silicn electrodes after cycling. Before XPS and TOF-SIMS tests, the electrodes were washed with a dimethyl carbonate (DMC) solvent. The mechanical performance tests were done through Atomic Force Microscopy (AFM, BRUKER Dimension FastScan) and a universal peeling testing machine (CRE-8007B). During the AFM tests, the probe was applied with an external force of 160 nN.

2.3. Electrochemical measurement

The coin cells were assembled in an Ar filled glovebox with oxygen and water contents less than 1 ppm using metallic lithium foil as the counter electrode. The electrolyte is composed of 1 M $LiPF_6$ and EC/DMC (1:1), containing 5 v/v% FEC. The ether-based electrolyte was 1 M LiTFSI in a well-mixed solution of DME/DOL (1:1 v/v). Cyclic voltammetry measurement was carried out on a versatile multichannel potentiostation 3/Z (VMP3) between 0.01 and 1.50 V at a scan rate of 0.1 mV s^{-1}. Galvanostatic intermittent titration technique (GITT) tests were also conducted on an NEWARE battery tester at room temperature in the voltage range of 0.01–1.5 V. Specifically, a constant current of 100 mA g^{-1} was applied to the battery for 30 min during the charge/discharge process, and then the current was interrupted for 2 h to make the battery reach a balanced state. The electrochemical impedance spectroscopy (EIS) was performed using the multichannel potentiostat 3/Z (VMP3) in the frequency range from 0.01 Hz to 1 × 10^5 Hz. Electrochemical cycling was conducted using an NEWARE battery test station. For full batteries, $LiFePO_4$ was used as the cathode, and the mass ratio of $LiFePO_4$, PVDF binder, and conductive carbon was 8:1:1 with N-Methyl-2-pyrrolidone (NMP) as a solvent. The slurry was evenly coated on an aluminum foil current collector. The Si@ 25-PU electrode was cycled for five cycles in a half-cell for pre-lithiation before being assembled into full cells. The corresponding mass loading of $LiFePO_4$ cathode is 12.0–14.0 mg cm^{-2} in order to achieve capacity matching with the Si@ 25-PU electrode. And the charge-discharge voltage range of the full cell is 2.5 V~4.1 V. The areal capacity ratio of Si@ 25-PU and $LiFePO_4$ electrode is controlled to be ~1.1. The electrolyte is composed of 1 M $LiPF_6$ and EC/DMC (1:1), containing 5 v/v% FEC. All electrochemical measurements were carried out at room temperature.

3. Results and discussion

3.1. Fabrication and characterization of artificial polyurea interface

Polyurea is selected as an artificial polymer interface due to existing numerous hydrogen bonds and polar functional groups, which contribute to the strong adhesion with silicon surface and the lithium ion transport dynamics [27,28]. A molecule-level uniform and controllable polyurea layer on the silicon electrode was achieved through MLD. A schematic diagram of the preparation process is displayed in Fig. 1a. The polyurea growth is based on the self-limiting reaction of two bifunctional organic precursors of 1, 4-phenylene diisocynaate (PDIC) and ethylenediamine (ED) [27]. The hydroxyl-terminated surface of silicon nanoparticles reacts with PDIC to obtain an isocyanate-terminated surface as depicted in Step 1, which subsequently reacts with ED to form the urea linkage as shown in Step 2. Then PDIC reacts with ED in turn in Step 3. The two sequences of Step 2 and Step 3 compose a single binary cycle. The conformal polyurea coating can be fabricated by repeating this binary cycle to obtain the desired thickness. Additionally, compared to

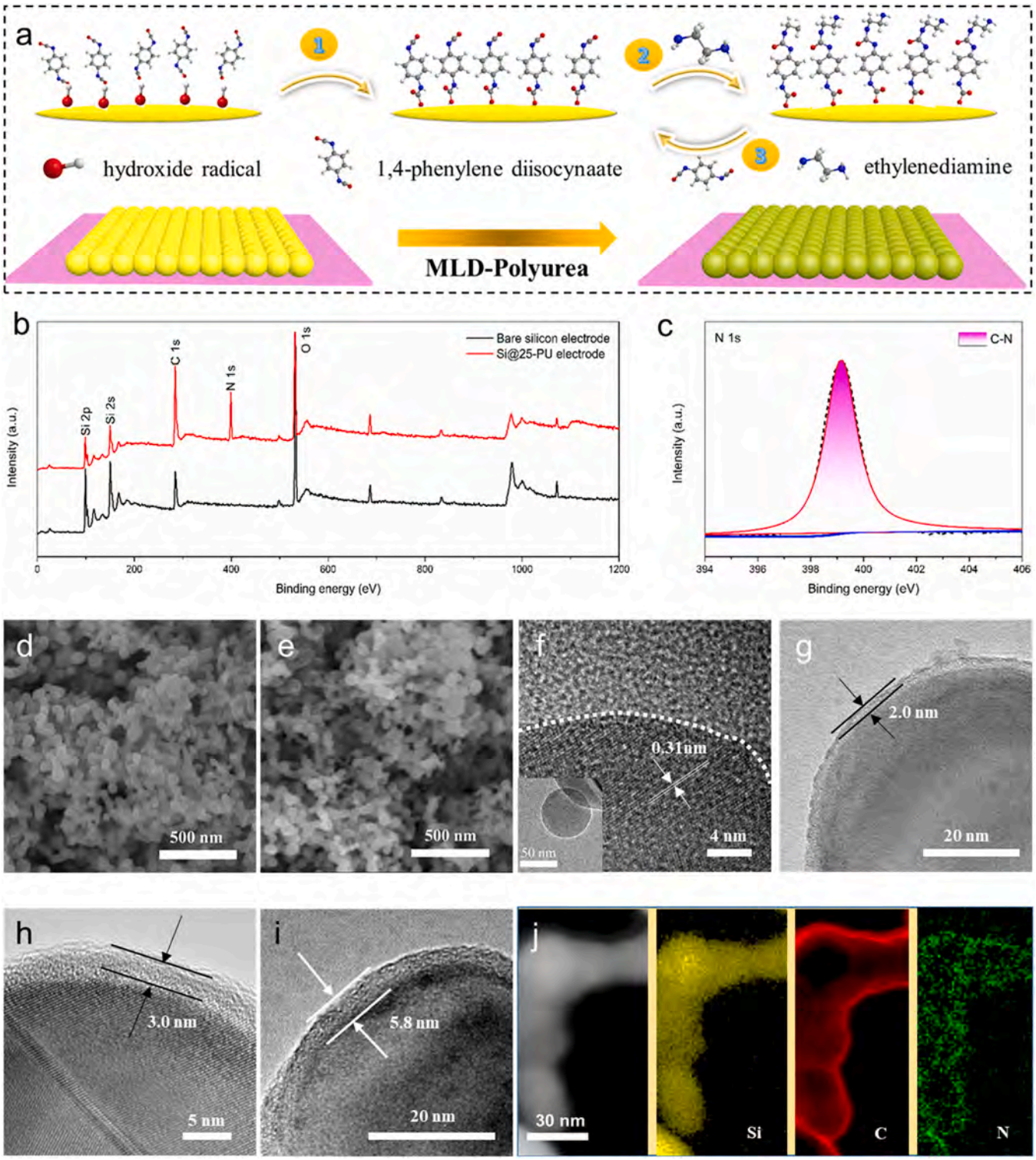

Fig. 1. (a) The preparation process diagram of the MLD-polyurea coated silicon electrode; XPS spectra (b) The XPS full spectra; (c) N1s XPS spectra; SEM images (d) Bare silicon electrode; (e) Si@ 25-PU electrode; HRTEM images (f) Bare silicon; (g) Si@ 15-PU; (h) Si@ 25-PU; (i) Si@ 50-PU; (j) The corresponding STEM-EELS mapping of Si@ 25-PU.

directly depositing on particles, the directly depositing on electrodes has significant advantage, since the deposition on the electrode can greatly reduce the effect of the deposited layer on the electron transport in the electrode scale [16,29]. Three sets of polyurea coatings with 15, 25, and 50 cycles were prepared and marked as Si@ 15-PU, Si@ 25-PU, and Si@ 50-PU electrode, respectively.

The X-ray photoelectron spectroscopy (XPS) full-spectra of Si@ 25-PU and bare silicon electrode are almost identical, except for the evident peak at ~400 eV as shown in Fig. 1b. This peak is attributed to the N 1 s peak of the characteristic C-N bond from polyurea polymer in Fig. 1c [28,30–32]. At the same energy position, no peak was observed for bare silicon electrode in Fig. S1. Meanwhile, the Si 2p peak shows that the silicon nanoparticles contain a natural oxide surface layer in Fig. S2a, facilitating the initiation of MLD deposition. After MLD deposition, no

significant change was observed in the Si 2p peak for the Si@ 25-PU electrode as shown in Fig. S2b. Therefore, the XPS spectra strongly prove the successful deposition of polyurea coating on the Si@ 25-PU electrode. Additionally, the Fourier-transform infrared spectrum of the simultaneously deposited polyurea film was characterized as shown in Fig. S3, and abundant polar functional groups (-HN-C═O, -NH) of polyurea layer are detected, which is conducive to the uniform and fast lithium ions diffusion at the electrolyte-electrode interface.

Further, scanning electron microscopy (SEM) was utilized to characterize the morphology of different electrodes. The SEM images of Si@ 25-PU electrode in Fig. 1e have no obvious difference with that of bare silicon electrode in Fig. 1d, reflecting the conformity and uniformity of the polyurea coating in the electrode. The Si@ 15-PU and Si@ 50-PU electrodes show similar conformal property in Fig. S4, which is determined by the unique advantage of MLD. Furthermore, the XRD spectra of bare silicon electrode and Si@ 25-PU electrode are almost the same as shown in Fig. S5, displaying the polyurea coating may be amorphous. Further, transmission electron microscopy (TEM) was performed to explore the thickness of artificial polyurea coatings. The size of silicon nanoparticles is mainly distributed in less than 80 nm as shown in Fig. S6a, and the corresponding diffraction rings are consistent with the characteristic rings of polycrystalline silicon in Fig. S6b. The HRTEM images of bare silicon nanoparticle is demonstrated in Fig. 1f, and the oxide layer on the particle surface is so thin that difficult to distinguish. The lattice fringe of 0.31 nm corresponds to the (111) plane of crystal silicon [33]. The uniform polyurea coatings can be clearly observed as

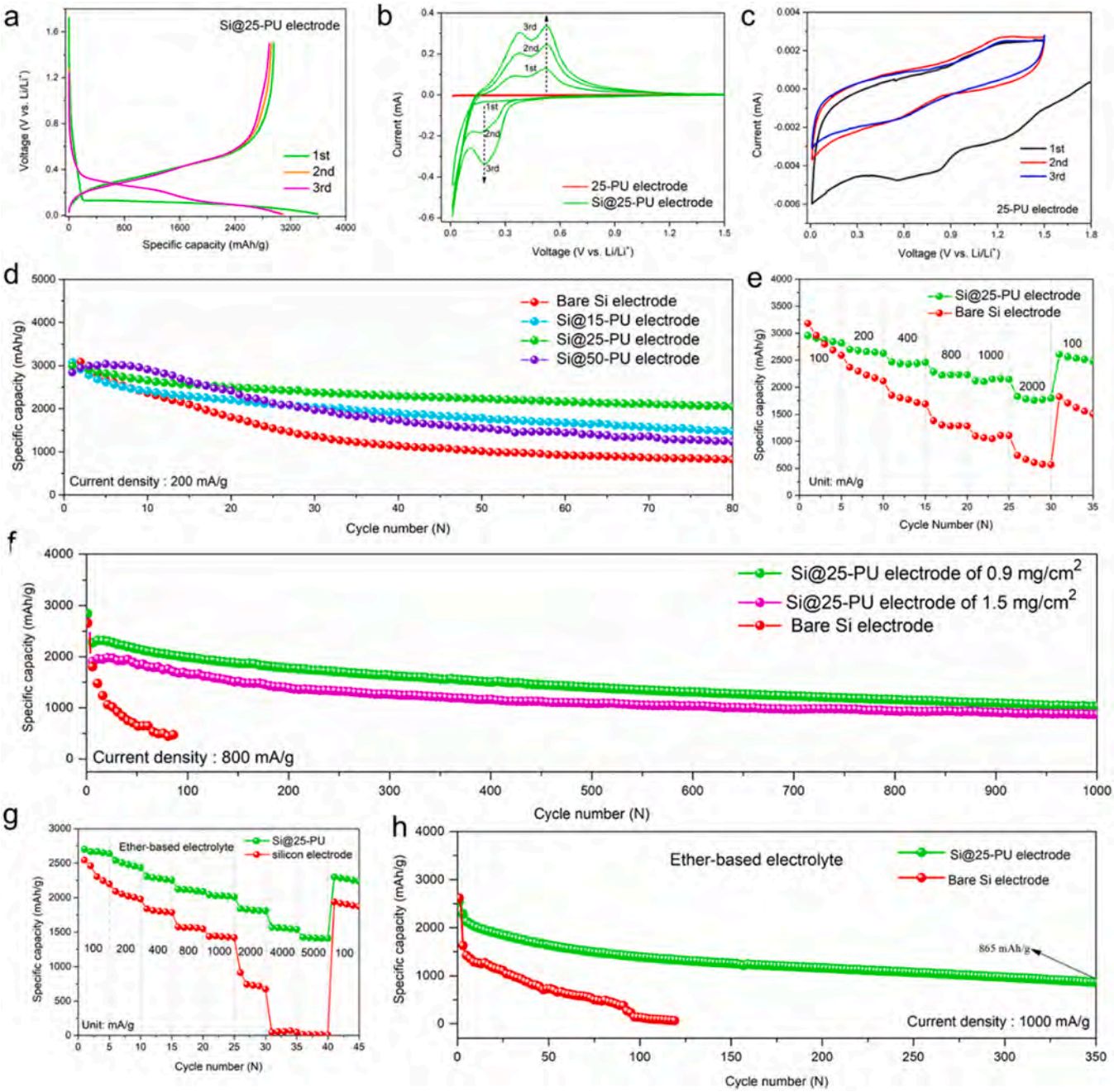

Fig. 2. The electrochemical performance (a) The initial three charge-discharge curves of Si@ 25-PU electrode; (b) CV curves of Si@ 25-PU and polyurea coating; (c) The enlarge CV curves of polyurea film; (d) The cycling stability at 200 mA g^{-1}; (e) The rate capability; (f) The long cycling performance under different loadings at 0.8 A g^{-1}. In ether-based electrolytes (g) The rate capability; (h) The long cycling performance at 1 A g^{-1}.

shown in Fig. 1g–i, which directly confirms the successful deposition of MLD polyurea. The polyurea coating thicknesses of Si@ 15-PU, Si@ 25-PU, Si@ 50-PU are 2.0, 3.0, and 5.8 nm, respectively. In Fig. 1j, the corresponding STEM-EELS mappings of elements (Si, C, N) also verify the uniform distribution of polyurea layers on silicon nanoparticles.

3.2. Electrochemical performance evaluation in half cells

The lithium storage performance of different silicon electrodes was characterized in half cells using different electrolyte systems (Fig. 2). In carbonate-based electrolyte, the polyurea coatings can significantly improve the initial Coulombic efficiency from 74% to $>81\%$ for different silicon electrodes as shown as Figs. 2a and S7. Specifically, the first coulombic efficiencies are 82.8% for Si@ 15-PU electrode, 82.3% for Si@ 25-PU electrode, and 81.3% for Si@ 50-PU electrode, respectively. This is mainly because the polyurea layer effectively prevents direct contact between the silicon and the liquid carbonate electrolyte and alleviates the side reactions during alloying/ dealloying process [16]. The initial three charge curves of Si@ 25-PU electrode display negligible capacity decay in Fig. 2a, implying excellent electrochemical reversibility. The cyclic voltammetry (CV) curves of Si@ 25-PU reflect the electrochemical characteristics of crystalline silicon during alloying/dealloying in Fig. 2b, and the bare silicon electrode exhibits consistent electrochemical behavior in Fig. S8. The CV test of polyurea film on copper foil was carried out as shown in Fig. 2b. Specifically, the sharp peak below 0.05 V in the first negative sweep represents the lithiation process of crystalline silicon anode. And the two reduction peaks at 0.18 V and ~0.02 V from the second cycle attribute to lithiation process of amorphous silicon. Correspondingly, the oxidation peaks at 0.33 V and 0.53 V belong to the dealloying process of the Li_xSi phase. Compared with the peak intensity of Si@ 25-PU, the peak intensity of pure polyurea film was negligible, indicating that the capacity contribution from polyurea coating is ignored [34]. An enlarged CV curve of polyurea film is shown in Fig. 2c. The CV curves after the first negative scan have little difference, demonstrating the good electrochemical stability of polyurea film.

The cycling stability is one of the most important parameters for evaluating the service life of silicon anodes. The cycling stability of different electrodes were tested at 200 mA g^{-1} as shown in Fig. 2d. The Si@ 25-PU electrode displays the best electrochemical cycling reversibility. A high reversible capacity of 2049 mA h g^{-1} was obtained after 80 cycles, and the corresponding capacity retention is up to 69%. By contrast, the reversible capacity of the bare silicon electrode is decayed to 792 mA h g^{-1}, and the corresponding capacity retention is only 26%. Therefore, the 25 cycles MLD polyurea corresponds to the optimal coating thickness (~3 nm) for balancing ion-electron transport ability and mechanical structural stability. Specifically, the too thin coating is disadvantageous for maintaining structural stability, while the too thick coating will hinder electron-ion transport and cause a huge electrochemical impedance. Furthermore, the cycling stability of the other silicon electrodes has been improved to varying degrees. The capacity retention is 47.98% for Si@ 15-PU electrode and 43.40% for Si@ 50-PU electrode, respectively. Besides, the corresponding Coulombic efficiency curves of Si@ 25-PU electrode and bare Si electrode are shown in Fig. S9. In the first 40 cycles, the Si@ 25-PU electrode shows a more stable Coulombic efficiency curve compared to bare silicon electrode, demonstrating the stabilizing effect of the polyurea layer on the electrode-electrolyte interface. Simultaneously, the Si@ 25-PU electrode shows significantly improved rate capability compared to the bare silicon electrode in Fig. 2e. Even at 2.0 A g^{-1}, a high reversible capacity of 1820 mA h g^{-1} is still maintained. As a comparison, the reversible capacity of the bare silicon electrode is only 600 mA h g^{-1} at 2.0 A g^{-1}. Moreover, the long-term cycling stability of Si@ 25-PU electrodes under different mass loadings of 0.9 mg cm^{-2} and 1.5 mg cm^{-2} was examined at 800 mA g^{-1} as displayed in Fig. 2f. The reversible capacities at 0.9 mg cm^{-2} and 1.5 mg cm^{-2} after 1000 cycles were 1010 mA h g^{-1} and 988 mA h g^{-1}, respectively. By contrast, the specific capacity of the bare silicon electrode decreased rapidly to 400 mA h g^{-1} after 100 cycles. And the corresponding Columbic efficiency curves are displayed in Fig. S10. Therefore, the Si@ 25-PU electrode demonstrates outstanding cycling stability and rate capability. The improved lithium storage performance benefits from the robust polyurea coating with favorable mechanical stability and electrochemical stability, which greatly enhances the structure and interface stability of silicon electrodes.

As is well-known, the larger size silicon particles have a lower cost and are easier for large-scale preparation. However, the poor structural stability caused by huge stress severely limits the cycling stability [35,36]. Two electrodes were prepared by using large-sized silicon particles of 150 nm and 230 nm, respectively. These two electrodes were deposited with 25 cycles MLD polyurea coating. SEM images of the corresponding silicon particles are shown in Figs. S11 and S12, respectively. For the polyurea coated 150 nm silicon electrode, a reversible capacity of 1513 mA h g^{-1} is obtained after 90 cycles in Fig. S13. For the polyurea coated 230 nm silicon electrode, a comparably high reversible capacity of 500 mA h g^{-1} is obtained after 50 cycles in Fig. S14. The cycling stability is significantly improved compared to the corresponding bare silicon particles, indicating the polyurea coating is effective for large-sized silicon particles.

Besides, the lithium storage performance of silicon anodes in the ether-based electrolytes is of importance for developing high energy density silicon-sulfur battery systems [37,38]. The first charge-discharge curve of the Si@ 25-PU electrode was tested at 100 mA g^{-1} in ether-based electrolytes as shown in Fig. S15. A high initial Coulombic efficiency of 82.5% is obtained. Moreover, the polyurea coating boosts impressive rate capability as displayed in Fig. 2g. Even at 5.0 A g^{-1}, a high reversible capacity of 1420 mA h g^{-1} is obtained. By comparison, the bare silicon electrode has virtually no capacity at 5.0 A g^{-1}. The corresponding charge-discharge curves of Si@ 25-PU electrode are exhibited in Fig. S16. Meanwhile, the Si@ 25-PU electrode displays outstanding cycling stability of 865 mA h g^{-1} after 350 cycles at 1 A g^{-1}. In contrast, the bare silicon electrode fails soon after 100 cycles in Fig. 2h. And the corresponding Columbic efficiency curves are displayed in Fig. S17. The Coulombic efficiencies of Si@ 25-PU electrode reached more than 98% after 10 cycles and are generally higher than that of bare silicon electrodes within the first 80 cycles. Besides, the corresponding Columbic efficiency curves of Si@ 25-PU electrode are smooth during 350 cycles, indicating that the polyurea layer can promote the formation of stable interfaces in ether-based electrolytes. In contrast, the Coulombic efficiency of bare silicon electrode curve exhibits obvious fluctuations, indicating an unstable interface. Therefore, the polyurea coating shows outstanding compatibility with the ether-based electrolytes. The above-mentioned superior lithium storage performance thanks to a robust artificial polyurea layer, which endows the exceptional electrochemical reversibility of silicon anodes.

3.3. Electrochemical kinetic evaluation of electrodes

Lithium ion transport in the electrodes is a critical factor affecting electrochemical stability and rate performance. Therefore, the effect of polyurea interface on the lithium ion diffusion kinetics of silicon electrodes was further explored to explain the improved electrochemical reversibility. The CV tests at different scan rates from 0.1 to 1.0 mV s^{-1} were performed to qualitatively analyze electrochemical kinetic as shown in Fig. 3a and b. As the scan rate increases, the intensity of cathodic and anodic peaks gradually increases. According to the Randles–Sevcik equation [39], the relationship between the apparent lithium ion diffusion coefficient in the electrode and the peak current can be expressed by the following formula:

$$I_p = SD^{1/2}\,\nu^{1/2}$$

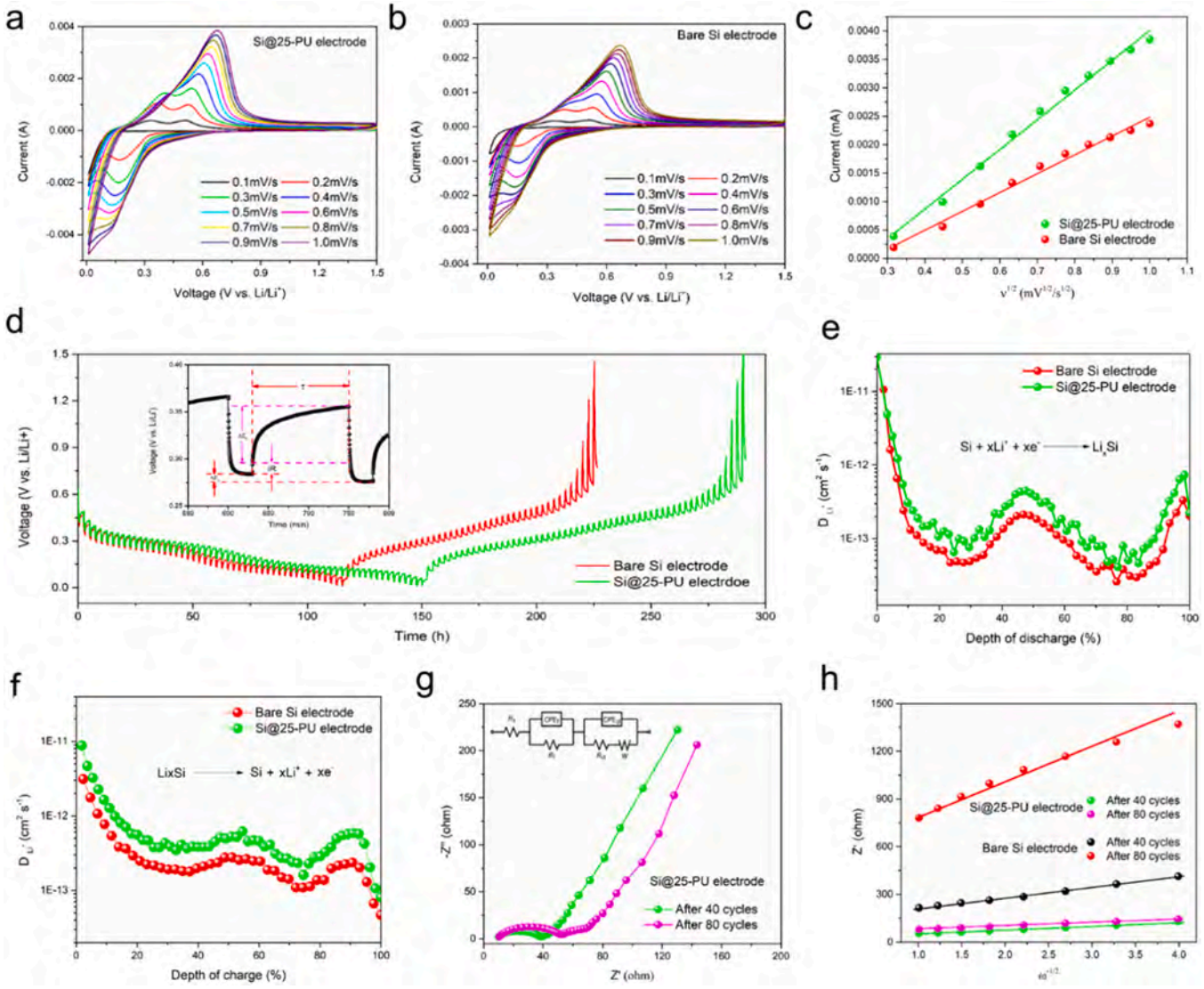

Fig. 3. The lithium ion transport kinetic evaluation. The CV curves at different scan rates (a) Si@ 25-PU; (b) Bare silicon electrode; (c) The linear relationship between the cathodic peak current (I_p) and the square root of the scan rate ($\nu^{1/2}$) for Si@ 25-PU and bare Si electrodes; (d) GITT curves of Si@ 25-PU electrode and bare Si electrode (the inset is the enlarge image for a single step of a GITT titration); The lithium ion diffusion coefficients (D_{Li}^{+}) of Si@ 25-PU and bare silicon electrodes (e) During lithiation processes; (f) During delithiation processes; (g) The EIS spectra of Si@ 25-PU electrode after 40 and 80 cycles; (h) The relationship between Z′ and $\omega^{-1/2}$ at the low frequency region.

In this formula, I_p is the peak current, and S is a battery-related constant, and D is the apparent lithium ions diffusion coefficient, and ν is the scan rate. The apparent lithium ion diffusion coefficient can be evaluated through a linear relationship between the cathodic peak current (I_p) and the square root of the scan rate ($\nu^{1/2}$). The corresponding linear fitting data are shown in Table S1. The line slope has a positive correlation with the lithium ion diffusion coefficient. Herein, the easily distinguishable oxidation peak at ~0.5 V is selected as the research object. The fitted linear relationship is shown in Fig. 3c. The Si@ 25-PU electrode shows a larger slope than bare silicon electrode, indicating faster lithium ion diffusion and more favorable electrochemical reaction kinetics for this dealloying process.

Further, the lithium ions diffusion ability at different charge-discharge states was quantitatively evaluated by galvanostatic intermittent titration technique (GITT). The specific lithium ion diffusion coefficient (D_{Li}^{+}) can be calculated by the following formula:

$$D_{Li^+} = \frac{4}{\pi\tau}\left(\frac{m_B V_m}{M_B S}\right)^2 \left(\frac{\Delta E_S}{\Delta E_\tau}\right)^2$$

In this formula, m_B, M_B, and V_m are the mass, molar mass, and molar volume of active materials in the electrodes, respectively. τ is the galvanic titration time. S is the surface area of the electrode. ΔE_S represents the steady-state voltage variation during a single GITT titration. ΔE_τ is the total voltage variation during a galvanic titration time. Fig. 3d shows the GITT curves of Si@ 25-PU electrode and bare silicon electrode after 10 cycles at 100 mA g^{-1}. ΔE_S and ΔE_τ can be obtained from a single step of a GITT titration as displayed in the inset of Fig. 3d. The D_{Li}^{+} of Si@ 25-PU electrode is higher than that of bare silicon electrode during alloying/dealloying processes as shown in Fig. 3e and f, further confirming that the conformal polyurea coating can promote the lithium ion diffusion kinetics. Additionally, the lithium ion diffusion kinetics after prolonged electrochemical cycles were characterized by electrochemical impedance spectroscopy (EIS). The EIS spectra of Si@ 25-PU electrode after 40 and 80 cycles are shown in Fig. 3g. The corresponding EIS spectra of bare silicon electrode are demonstrated in Fig. S18. Obviously, the EIS spectra include two semicircles at mid/high frequency regions and a straight line at low frequency region, representing the interface impedance (R_{SEI}), charge transfer resistance (R_{ct}), and

lithium ion diffusion impedance (Z_w), respectively [40,41]. And Z′ (real part of impedance) has a linear relationship with the negative square root of the angular frequency ($\omega^{-1/2}$) as shown in Fig. 3h. According to previous reports, the slope of the fitted line is negatively correlated with the lithium ion diffusion coefficient [42]. In other words, the smaller the slope, the larger the lithium ion diffusion coefficient. The statistics graph of the fitted slopes after different cycles are shown in Fig S19. The Si@ 25-PU electrode maintains a faster lithium ion diffusion than bare silicon electrode no matter after 40 or 80 cycles. Besides, as the cycle goes on, the lithium ion diffusion ability of Si@ 25-PU electrode did not change significantly, while the reaction kinetics of bare silicon electrode deteriorated obviously, indicating that the polyurea coating still can promote the electrode reaction kinetics after many cycles. The improved lithium ion diffusion kinetics stems from numerous polar functional groups and abundant hydrogen bonds in the intrinsic polyurea structure, which is conducive to the adsorption and transfer of lithium ions. Additionally, the enhanced electrode integrity and structural stability by the polyurea coating is also an important reason for the accelerated reaction kinetics.

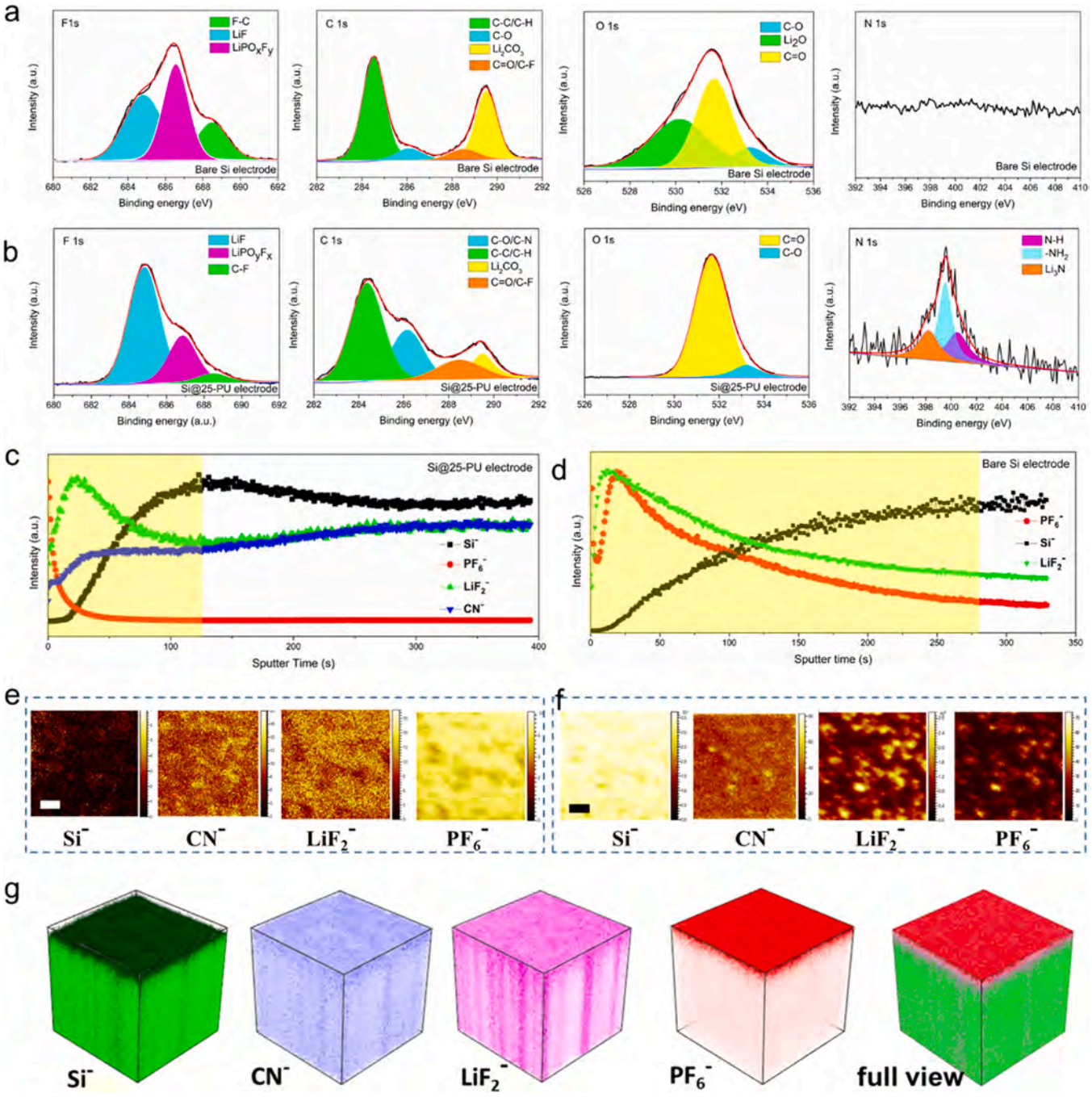

Fig. 4. XPS spectra of different elements for post-cycled electrodes (a) Bare silicon electrode; (b) Si@ 25-PU electrode; Normalized depth profiles via TOF-SIMS measurements after 50 cycles (c) Si@ 25-PU electrode; (d) Bare silicon electrode. The TOF-SIMS secondary ion images of Si@ 25-PU electrode after Cs^+ consecutive sputtering (e) After 30 s; (f) After 380 s (g) The 3D view images of the sputtered volume corresponding to the depth profiles in (c). (The length of scale bar is 25 μm.).

3.4. Interface analysis of post-cycled electrodes

As an artificial SEI, it is critical to understand the influence of polyurea coating on the interface stability of silicon anodes. According to the EIS spectra in Figs. 3g and S18, the fitted R_{SEI} is counted in Fig. S20. For bare silicon electrode, the R_{SEI} has a larger value and shows a dramatic increase from 103 to 256 Ω. By contrast, the R_{SEI} of Si@ 25-PU electrode displays a slight increase from 24 to 34 Ω, indicating that the artificial polyurea coating can significantly reduce the interface impedance and promote the formation of a stable SEI. Furthermore, the components of the SEI were analyzed to gain a deep understanding of the interface chemistry affected by polyurea coating. XPS was applied to detect the SEIs for Si@ 25-PU electrode and bare silicon electrode after 50 cycles. The XPS peaks of different elements are shown in Fig. 4a and b. Examining F 1 s, the peak at ~684.5 eV corresponding to LiF significantly increases for the Si@ 25-PU electrode, indicating the proportion of LiF is increased compared to that of bare silicon electrode. This manifests the polyurea layer can promote the formation of LiF in the carbonate-based electrolyte, which shows similar conclusions in lithium metal anode research [30]. According to previous reports, LiF is an important component of a stable SEI due to the high elastic modulus and ionic conductivity [22,30,43,44]. Regarding the increasing proportion of LiF, there are two possible reasons. One is that the polyurea coating can effectively reduce the $LiPO_yF_x$ produced by the decomposition of the lithium salts [45]. Specifically, the polyurea coating effectively prevents pulverization of silicon particles, thereby inhibiting the more decomposition of the lithium salt on the fresh silicon surface. The other possible reason is that the polyurea coating changes the SEI-generated reaction pathways and induces the formation of more LiF from the decomposition of FEC or lithium salt. The C 1 s peak contribution corresponding to Li_2CO_3 is also weakened for the Si@ 25-PU electrode, suggesting that the polyurea coating inhibits the formation of insoluble electrolyte reduction products [22,46]. Additionally, a possible reason is that the polyurea layer effectively inhibits the electrochemical decomposition of the solvent (EC) on the silicon surface, blocks the formation of lithium ethylene dicarbonate, and reduces the generation of Li_2CO_3 [47,48]. For O1s spectra, the Li_2O content in SEIs of Si@ 25-PU is significantly reduced compared to bare silicon electrodes, suggesting the polyurea coating can reduce the proportion of Li_2O. Recent studies have shown that the Li_2O in SEI is most likely from the decomposition of EC, rather than the conversion of the surface oxide layer of the silicon anode [49–51]. Similarly, the inhibited electrochemical decomposition of the solvents by polyurea layer is one of the possible reasons for the reduced Li_2O content. Finally, the N 1 s peak contains three peaks, corresponding to 400.5 eV (N-H), 399.5 eV (O═C–NH–) and 398.2 eV (Li_3N), respectively [28,52]. Li_3N is most likely the reduction product of polyurea coating and is beneficial to lithium ion transport. For contrast, there is not any peak for bare silicon electrode. Therefore, the polyurea coating promotes the formation of a LiF-rich SEI on the silicon electrodes. Note that the underlying mechanism responsible of inducing LiF formation still need further research in our future work. Obviously, this LiF-dominated SEI is significant to achieving stable cycling performance and superior rate capability.

The SEI thickness and structure of Si@ 25-PU electrode were further evaluated by time-of-flight secondary ion mass spectrometry (TOF-SIMS). We can evaluate the SEI thickness by correlating the sputter time to the change in fluoride and silicon signals, identifying when the fluoride rich SEI ends and the Si bulk begins [53]. In Fig. 4c and d, the signals of Si^- and LiF_2^- represent the silicon and LiF, and the PF_6^- comes from $LiPO_xF_y$ or residual $LiPF_6$, and the CN^- origins from the polyurea coating. Evidently, the corresponding sputter time of Si@ 25-PU electrode (~120 s) is shorter than that of bare silicon electrode (~270 s), displaying the Si@ 25-PU electrode has a thinner SEI. This can explain why the R_{SEI} of Si@ 25-PU electrode is so much smaller. Additionally, the CN^- signal soon reaches steady state during sputtering, indicating the polyurea coating is evenly distributed inside the silicon electrode.

The corresponding TOF-SIMS secondary ion images of Si@ 25-PU electrode after 30 s and 380 s are shown in Fig. 4e and f. The silicon signal is quite weak in Fig. 4e, showing the silicon electrode surface is covered by the SEI. After 380 s sputter, the silicon signal is saturated as shown in Fig. 4f, demonstrating the silicon is completely exposed. Surprisingly, the LiF signal appears in scattered bright spots, which is most likely caused by the porosity of electrodes. Simultaneously, the corresponding 3D reconstruction view images were performed as exhibited in Fig. 4g, which can intuitively show the Si@ 25-PU electrode structure after cycling. The LiF exhibits a columnar distribution in the electrode, which is consistent with the pore identification in Fig. 4f. Meanwhile, the uniform distribution of polyurea coating in the electrode can be confirmed. Combining the above-mentioned data, the polyurea layer can reduce the decomposition of lithium salt and promote the formation of a thinner, LiF-dominated SEI on Si@ 25-PU electrode.

3.5. Mechanical properties analysis and morphology of electrodes

The mechanical properties were evaluated to explore the effect of the polyurea coating on the structure stability of silicon electrodes. An 180° peeling test with 3 M tape was performed to evaluate the effect of polyurea on mechanical properties of silicon electrode before cycling as shown in Fig. S21. The results indicate that the Si@ 25-PU electrode provides an adhesive force (0.75 N) as displayed in Fig. 5a, which is twice as strong as that of the bare silicon electrode (0.37 N). This directly confirms that the polyurea can greatly enhance the mechanical stability of silicon electrode by strengthening the interaction between the components of the electrodes, including active materials, binders and current collectors, conductive carbon. The improved adhesion ability benefit from the large number of self-healing hydrogen bonds in polyurea structure [54]. For the cycled electrodes, the mechanical properties of the SEIs were explored by Atomic Force Microscope (AFM) tests. The representative force–displacement curves of the Si@ 25-PU electrode and bare silicon electrode after cycling are exhibited in Figs. 5b and S22, respectively. Similar curves indicate that the SEIs of Si@ 25-PU electrode and bare silicon electrode have the similar elastic mechanical behavior within the range of applied external force. However, Si@ 25-PU electrode generally has a higher average Young's modulus (~3.0 GPa) than that (~1.5 GPa) of bare silicon electrode based on sampling points, indicating that the polyurea coating promotes a compact and robust SEI. Selected seven groups of representative Young's modulus are exhibited in Fig. 5c. And the strong mechanical property boosted by the polyurea coating are directly related to the LiF-rich chemistry composition in SEIs.

The morphology evolution of electrodes was explored after cycling as shown in Fig. 5d and e. The visual integrity of Si@ 25-PU electrode can be perceived through digital photos. On the contrary, lots of active materials are detached from the current collector for the bare silicon electrode. Besides, the Si@ 25-PU electrode still shows an intact surface from the top view after 80 cycles. By contrast, the bare silicon electrode shows numerous obvious cracks, which will severely destroy the conductive network of the electrode. The comparison shows that the polyurea layer can greatly improve the structure integrity and stability of silicon electrode. Meanwhile, the thickness increase of the Si@ 25-PU electrode is significantly reduced (68.7%) relative to the bare silicon electrode (118.7%) from the cross-section views in Fig. 5f and g. After 500 and 1000 cycles, the Si@ 25-PU electrode shows a smooth and flat surface in Fig. S23a and b. Some cracks can be observed due to the inevitable volume swelling during long-term cycling. Unexpectedly, a stretched elastic film was observed at the cracks, potentially preventing the cracks from expanding further or becoming completely detached, maintaining structural stability and integrity of electrodes. Consequently, the conformal polyurea coating endows the silicon electrode more excellent mechanical properties, which is essential to maintain the structural stability of electrode and long cycle life of batteries.

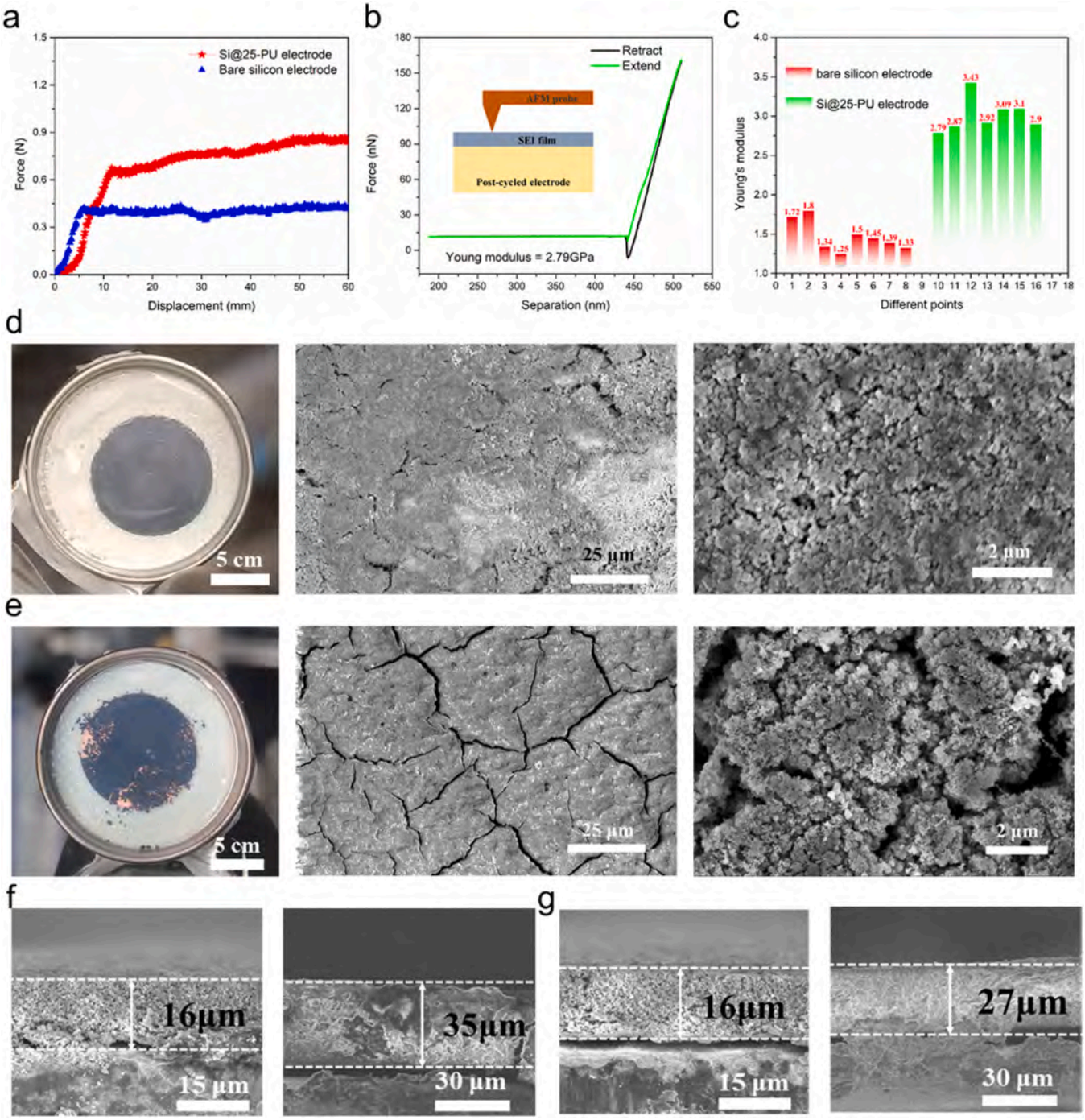

Fig. 5. (a) Force–displacement curves of Si@ 25-PU electrode and bare silicon electrode; (b) The representative force–displacement curve from AFM for Si@ 25-PU electrode after 80 cycles; (c) Young's modulus statistics; Digital photos and SEM images of electrodes after 80 cycles (d) Si@ 25-PU; (e) Bare silicon electrode; Cross-section views of electrodes before and after 80 cycles (f) Bare silicon electrode; (g) Si@ 25-PU electrode.

3.6. *Full-cell performance and polyurea-driven performance superiority*

To confirm the applicability of Si@ 25-PU electrode, the $LiFePO_4$//Si@ 25-PU full cells were designed and assembled. Fig. 6a shows the structure schematic diagram of the $LiFePO_4$//Si@ 25-PU full cell. The commercial $LiFePO_4$ cathode shows excellent electrochemical performance in half-cells as shown in Fig. S24, including high first Columbic efficiency (99.4%) and excellent capacity retention (100.8%after 35 cycles). It is important to note that the Si@ 25-PU electrode is electrochemically pre-lithiated in a half-cell to obtain the high initial Coulombic efficiency. The first charge-discharge curve of the full cell is exhibited in Fig. 6b, and the corresponding Columbic efficiency is 94.7%, which is highly comparable to commercial graphite-based full batteries [41,55]. Based on the total mass of cathode and anode, the energy density of the full cells reaches as high as 453.0 Wh kg^{-1}. The 100th charge-discharge curve of full cell is displayed in Fig. S25, and the corresponding energy density is 376.0 Wh kg^{-1}, exhibiting good capacity retention of 83.0%. The charge-discharge curves of full cell at different rates are shown in Fig. 6c. The outstanding rate capability and cycling stability were demonstrated in Fig. 6d. Specifically, a high reversible capacity of 121 mA h g^{-1} was maintained at 1 C (1 C = 155 mA g^{-1}), and a high capacity of 125 mA h g^{-1} was

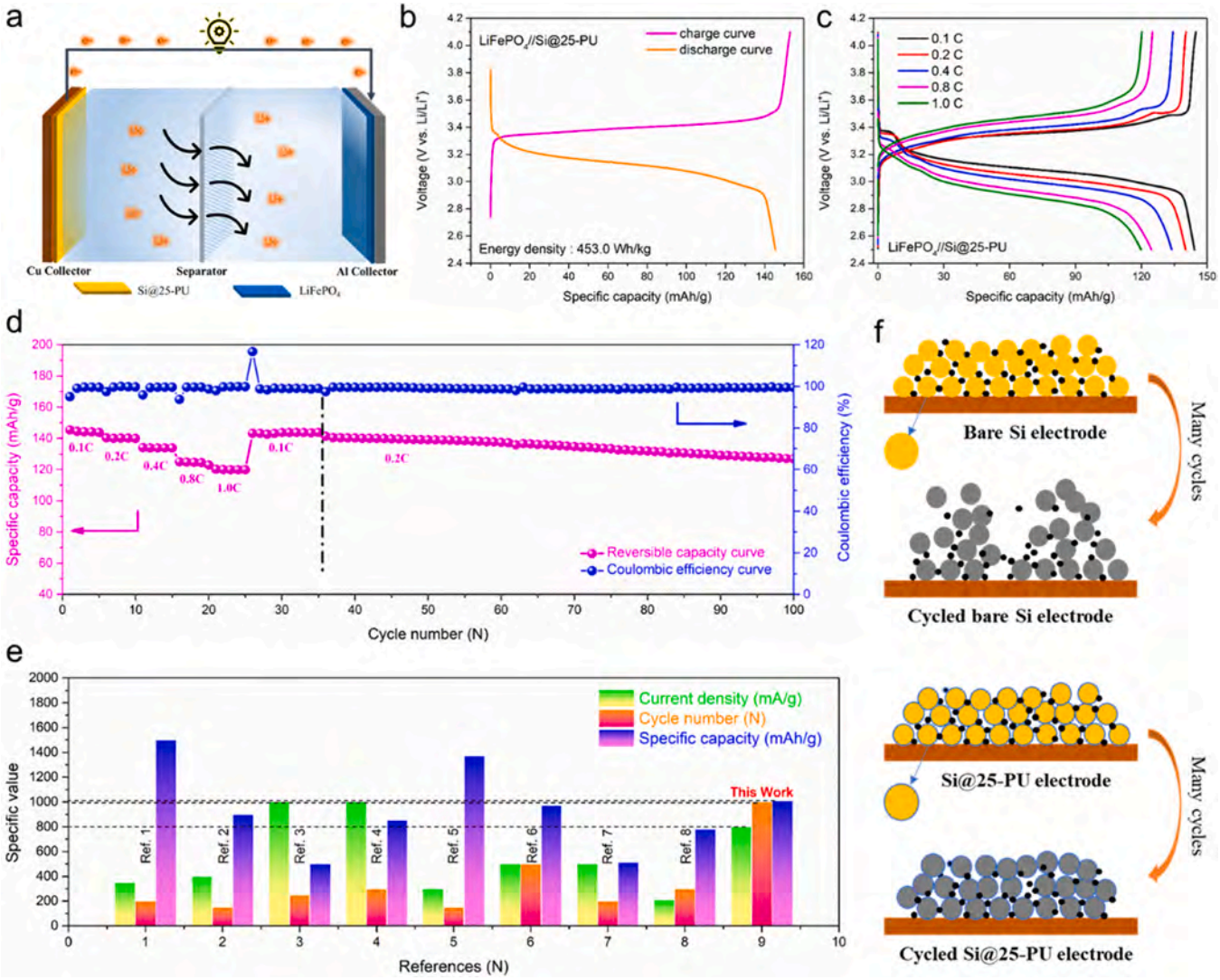

Fig. 6. (a) A schematic diagram of the $LiFePO_4$//Si@ 25-PU full cell; (b) The initial charge-discharge curve of the full cell; (c) The rate charge-discharge curves; (d) The rate capability and cycling stability of the full cell; (e) Comprehensive comparison with recent some similar works in terms of current density, cycle life, and specific capacity; (f) A schematic diagrams of the structural evolution before and after cycling for bare silicon electrode and Si@ 25-PU electrode.

maintained after 100 cycles. The impressive electrochemical performance of full cells further confirms the great potential of Si@ 25-PU electrode in practical applications.

Additionally, some recent works on silicon anodes have been comprehensively compared from current density, cycle stability, and specific capacity as displayed in Fig. 6e. The detailed information of the corresponding references is shown in Table S2. Clearly, the polyurea gives the silicon anode a comprehensive performance advantage, even better than the electrochemical performance of some silicon-carbon composite anodes. Such outstanding electrochemical lithium storage performance benefits from a polyurea-derived LiF-dominated SEI with excellent mechanical stability, which can significantly improve the structural stability of silicon anode and the electrode integrity. Simultaneously, this conformal polyurea layer with polar functional groups greatly improves the lithium ion diffusion dynamics of silicon anodes during cycling. The polyurea-promoted electrode structural stability advantage is vividly shown in Fig. 6f.

4. Conclusion

In summary, an artificial polyurea layer with abundant polar functional groups and hydrogen bonds is successfully deposited on the silicon electrode via MLD. The optimal polyurea layer of ~3 nm greatly improves the electrochemical performance of silicon anodes, including a high initial Columbic efficiency (82.4%), outstanding rate capability (1820 mA h g^{-1} at 2 A g^{-1}), and long cycling stability (1010 mA h g^{-1} after 1000 cycles). This polyurea coating greatly improves the lithium ion transport dynamics in silicon electrode and promotes the formation of a robust, thin LiF-dominated SEI, which maintain the structural stability and integrity of electrodes. Furthermore, the $LiFePO_4$//Si@ 25-PU full battery shows outstanding cycling stability and achieves a high energy density of 453 Wh kg^{-1}. Meanwhile, the polyurea layer demonstrates good compatibility with larger-size silicon particles (even >150 nm) and the ether-based electrolytes (1420 mA h g^{-1} at 5 A g^{-1}, 865 mA h g^{-1} after 350 cycles). Therefore, the effective and robust artificial polyurea coating shows great promise in the practical application of silicon anodes.

CRediT authorship contribution statement

Tiansheng Mu designed the experimental plan; Geping Yin, Xueliang Sun, and Pengjian Zuo gave experimental guidance; Tiansheng Mu completed the experiment and collected data; Yipeng Sun, Changhong Wang, and Yang Zhao assisted in the mechanical property testing;

Jianneng Liang provided verification for the experimental phenomena; Xulei Sui and Ruying Li contributed to the data analysis; Tiansheng Mu and Kieran Doyle-Davis contributed to the writing and polishing of the article; Tiansheng Mu, Geping Yin, Chunyu Du, and Xueliang Sun provided resource support; All authors discussed the results and commented on the manuscript.

Declaration of Competing Interest

The authors declare that they have no known competing financial interests or personal relationships that could have appeared to influence the work reported in this paper.

Data availability

Data will be made available on request.

Acknowledgments

This work was supported by the Natural Science Foundation of China (No. 51634003) and China Postdoctoral Science Foundation (2022M710951, 2022TQ0087). This research was also supported by the Natural Sciences and Engineering Research Council of Canada (NSERC), the Canada Research Chair Program (CRC), the Canada Foundation for Innovation (CFI). Tiansheng Mu also acknowledges financial support from the China Scholarship Council (CSC).

Appendix A. Supplementary material

Supplementary data associated with this article can be found in the online version at doi:10.1016/j.nanoen.2022.107829.

References

[1] H. Jin, S. Xin, C. Chuang, W. Li, H. Wang, J. Zhu, H. Xie, T. Zhang, Y. Wan, Z. Qi, W. Yan, Y.-R. Lu, T.-S. Chan, X. Wu, J.B. Goodenough, H. Ji, X. Duan, Black phosphorus composites with engineered interfaces for high-rate high-capacity lithium storage, Science 370 (2020) 192–197.
[2] M. Ko, S. Chae, J. Ma, N. Kim, H.-W. Lee, Y. Cui, J. Cho, Scalable synthesis of silicon-nanolayer-embedded graphite for high-energy lithium-ion batteries, Nat. Energy 1 (2016) 16113.
[3] T. Mu, P. Zuo, S. Lou, Q. Pan, Q. Li, C. Du, Y. Gao, X. Cheng, Y. Ma, G. Yin, A two-dimensional nitrogen-rich carbon/silicon composite as high performance anode material for lithium ion batteries, Chem. Eng. J. 341 (2018) 37–46.
[4] B. Philippe, R. Dedryvere, M. Gorgoi, H. Rensmo, D. Gonbeau, K. Edstrom, Improved performances of nanosilicon electrodes using the salt LiFSI: a photoelectron spectroscopy study, J. Am. Chem. Soc. 135 (2013) 9829–9842.
[5] Y. Xu, K. Wood, J. Coyle, C. Engtrakul, G. Teeter, C. Stoldt, A. Burrell, A. Zakutayev, Chemistry of electrolyte reduction on lithium silicide, J. Phys. Chem. C 123 (2019) 13219–13224.
[6] B. Moeremans, H.W. Cheng, C. Merola, Q. Hu, M. Oezaslan, M. Safari, M.K. Van Bael, A. Hardy, M. Valtiner, F.U. Renner, In situ mechanical analysis of the nanoscopic solid electrolyte interphase on anodes of Li-ion batteries, Adv. Sci. 6 (2019), 1900190.
[7] J. Shin, T.-H. Kim, Y. Lee, E. Cho, Key functional groups defining the formation of Si anode solid-electrolyte interphase towards high energy density Li-ion batteries, Energy Storage Mater. 25 (2020) 764–781.
[8] K. Schroder, J. Alvarado, T.A. Yersak, J. Li, N. Dudney, L.J. Webb, Y.S. Meng, K. J. Stevenson, The effect of fluoroethylene carbonate as an additive on the solid electrolyte interphase on silicon lithium-ion electrodes, Chem. Mater. 27 (2015) 5531–5542.
[9] C. Xu, F. Lindgren, B. Philippe, M. Gorgoi, F. Björefors, K. Edström, T. Gustafsson, Improved performance of the silicon anode for Li-ion batteries: understanding the surface modification mechanism of fluoroethylene carbonate as an effective electrolyte additive, Chem. Mater. 27 (2015) 2591–2599.
[10] J.D. McBrayer, M.-T.F. Rodrigues, M.C. Schulze, D.P. Abraham, C.A. Apblett, I. Bloom, G.M. Carroll, A.M. Colclasure, C. Fang, K.L. Harrison, G. Liu, S. D. Minteer, N.R. Neale, G.M. Veith, C.S. Johnson, J.T. Vaughey, A.K. Burrell, B. Cunningham, Calendar aging of silicon-containing batteries, Nat. Energy 6 (2021) 866–872.
[11] Y. He, X. Yu, Y. Wang, H. Li, X. Huang, Alumina-coated patterned amorphous silicon as the anode for a lithium-ion battery with high coulombic efficiency, Adv. Mater. 23 (2011) 4938–4941.
[12] Y. Bai, D. Yan, C. Yu, L. Cao, C. Wang, J. Zhang, H. Zhu, Y.-S. Hu, S. Dai, J. Lu, W. Zhang, Core-shell Si@TiO 2 nanosphere anode by atomic layer deposition for Li-ion batteries, J. Power Sources 308 (2016) 75–82.
[13] D. Kim, M. Park, S.M. Kim, H.C. Shim, S. Hyun, S.M. Han, Conversion reaction of nanoporous ZnO for stable electrochemical cycling of binderless Si microparticle composite anode, ACS Nano 12 (2018) 10903–10913.
[14] C. Cao, I.I. Abate, E. Sivonxay, B. Shyam, C. Jia, B. Moritz, T.P. Devereaux, K. A. Persson, H.-G. Steinrück, M.F. Toney, Solid electrolyte interphase on native oxide-terminated silicon anodes for Li-ion batteries, Joule 3 (2019) 762–781.
[15] B. Zhu, N. Liu, M. McDowell, Y. Jin, Y. Cui, J. Zhu, Interfacial stabilizing effect of ZnO on Si anodes for lithium ion battery, Nano Energy 13 (2015) 620–625.
[16] C. Zhu, K. Han, D. Geng, H. Ye, X. Meng, Achieving high-performance silicon anodes of lithium-ion batteries via atomic and molecular layer deposited surface coatings: an overview, Electrochim. Acta 251 (2017) 710–728.
[17] Y. Zhao, X. Sun, Molecular layer deposition for energy conversion and storage, ACS Energy Lett. 3 (2018) 899–914.
[18] S. Zeng, D. Liu, Y. Chen, J. Qian, Y. Cao, H. Yang, X. Ai, Enabling a high capacity and long cycle life for nano-Si anodes by building a stable solid interface with a Li +-conducting polymer, J. Mater. Chem. A 3 (2015) 9938–9944.
[19] J.-J. Cai, P.-J. Zuo, X.-Q. Cheng, Y.-H. Xu, G.-P. Yin, Nano-silicon/polyaniline composite for lithium storage, Electrochem. Commun. 12 (2010) 1572–1575.
[20] J. Zhang, S. Fan, H. Wang, J. Qian, H. Yang, X. Ai, J. Liu, Surface-bound silicon nanoparticles with a planar-oriented N-type polymer for cycle-stable Li-ion battery anode, ACS Appl. Mater. Interfaces 11 (2019) 13251–13256.
[21] M.-S. Song, G. Chang, D.-W. Jung, M.-S. Kwon, P. Li, J.-H. Ku, J.-M. Choi, K. Zhang, G.-R. Yi, Y. Cui, J.H. Park, Strategy for boosting Li-ion current in silicon nanoparticles, ACS Energy Lett. 3 (2018) 2252–2258.
[22] B.H. Shen, S. Wang, W.E. Tenhaeff, Ultrathin conformal polycyclosiloxane films to improve silicon cycling stability, Sci. Adv. 5 (2019) eaaw4856.
[23] D. Bresser, D. Buchholz, A. Moretti, A. Varzi, S. Passerini, Alternative binders for sustainable electrochemical energy storage – the transition to aqueous electrode processing and bio-derived polymers, Energy Environ. Sci. 11 (2018) 3096–3127.
[24] Y. Liu, Y. Zhu, Y. Cui, Challenges and opportunities towards fast-charging battery materials, Nat. Energy 4 (2019) 540–550.
[25] S.B. Son, Y. Wang, J. Xu, X. Li, M. Groner, A. Stokes, Y. Yang, Y.T. Cheng, C. Ban, Systematic investigation of the alucone-coating enhancement on silicon anodes, ACS Appl. Mater. Interfaces 9 (2017) 40143–40150.
[26] Y. He, D.M. Piper, M. Gu, J.J. Travis, S.M. George, S.-H. Lee, A. Genc, L. Pullan, J. Liu, S.X. Mao, J.-G. Zhang, C. Ban, C. Wang, In situ transmission electron microscopy probing of native oxide and artificial layers on silicon nanoparticles for lithium ion batteries, ACS Nano 8 (2014) 11816–11823.
[27] Y. Chen, B. Zhang, Z. Gao, C. Chen, S. Zhao, Y. Qin, Functionalization of multiwalled carbon nanotubes with uniform polyurea coatings by molecular layer deposition, Carbon 82 (2015) 470–478.
[28] S.M.N. Uddin, Y. Nagao, Multilayer growth of porphyrin-based polyurea thin film using solution-based molecular layer deposition technique, Langmuir 33 (2017) 12777–12784.
[29] C. Ban, S.M. George, Molecular layer deposition for surface modification of lithium-ion battery electrodes, Adv. Mater. Interfaces 3 (2016).
[30] Y. Sun, Y. Zhao, J. Wang, J. Liang, C. Wang, Q. Sun, X. Lin, K.R. Adair, J. Luo, D. Wang, R. Li, M. Cai, T.K. Sham, X. Sun, A novel organic "polyurea" thin film for ultralong-life lithium-metal anodes via molecular-layer deposition, Adv. Mater. 31 (2019), e1806541.
[31] N.K.Chiaki INOUE, Mamoru ISHIGURO, Kazunaka ENDO, Analysis of microcapsule resin using the X-ray photoelectron nitrogen ls spectral method, Polym. J. 27 (1995) 651–654.
[32] I. Abdulazeez, O.C.S. Al-Hamouz, M. Khaled, A.A. Al-Saadi, Inhibition of mild steel corrosion in CO_2 and H2S-saturated acidic media by a new polyurea-based material, Mater. Corros. (2019).
[33] Q. Pan, P. Zuo, T. Mu, C. Du, X. Cheng, Y. Ma, Y. Gao, G. Yin, Improved electrochemical performance of micro-sized SiO-based composite anode by prelithiation of stabilized lithium metal powder, J. Power Sources 347 (2017) 170–177.
[34] S. Chen, L. Shen, P.A. van Aken, J. Maier, Y. Yu, Dual-functionalized double carbon shells coated silicon nanoparticles for high performance lithium-ion batteries, Adv. Mater. 29 (2017).
[35] B. Zhu, Y. Jin, Y. Tan, L. Zong, Y. Hu, L. Chen, Y. Chen, Q. Zhang, J. Zhu, Scalable production of Si nanoparticles directly from low grade sources for lithium-ion battery anode, Nano Lett. 15 (2015) 5750–5754.
[36] L. Luo, P. Zhao, H. Yang, B. Liu, J.G. Zhang, Y. Cui, G. Yu, S. Zhang, C.M. Wang, Surface coating constraint induced self-discharging of silicon nanoparticles as anodes for lithium ion batteries, Nano Lett. 15 (2015) 7016–7022.
[37] R. Mo, Z. Lei, D. Rooney, K. Sun, Anchored monodispersed silicon and sulfur nanoparticles on graphene for high-performance lithiated silicon-sulfur battery, Energy Storage Mater. 23 (2019) 284–291.
[38] B. Li, S. Li, J. Xu, S. Yang, A new configured lithiated silicon–sulfur battery built on 3D graphene with superior electrochemical performances, Energy Environ. Sci. 9 (2016) 2025–2030.
[39] T. Mu, S. Lou, N.G. Holmes, C. Wang, M. He, B. Shen, X. Lin, P. Zuo, Y. Ma, R. Li, C. Du, J. Wang, G. Yin, X. Sun, Reversible silicon anodes with long cycles by multifunctional volumetric buffer layers, ACS Appl. Mater. Interfaces 13 (2021) 4093–4101.
[40] Q. Pan, P. Zuo, S. Lou, T. Mu, C. Du, X. Cheng, Y. Ma, Y. Gao, G. Yin, Micro-sized spherical silicon@carbon@graphene prepared by spray drying as anode material for lithium-ion batteries, J. Alloy. Compd. 723 (2017) 434–440.
[41] T. Mu, Z. Zhang, Q. Li, S. Lou, P. Zuo, C. Du, G. Yin, Scalable submicron/micron silicon particles stabilized in a robust graphite-carbon architecture for enhanced lithium storage, J. Colloid Interface Sci. 555 (2019) 783–790.

[42] T. Mu, B. Shen, S. Lou, Z. Zhang, Y. Ren, X. Zhou, P. Zuo, C. Du, Y. Ma, H. Huo, G. Yin, Scalable mesoporous silicon microparticles composed of interconnected nanoplates for superior lithium storage, Chem. Eng. J. 375 (2019), 121923.
[43] S. Liu, X. Ji, J. Yue, S. Hou, P. Wang, C. Cui, J. Chen, B. Shao, J. Li, F. Han, J. Tu, C. Wang, High interfacial-energy interphase promoting safe lithium metal batteries, J. Am. Chem. Soc. 142 (2020) 2438–2447.
[44] J. Zhao, L. Liao, F. Shi, T. Lei, G. Chen, A. Pei, J. Sun, K. Yan, G. Zhou, J. Xie, C. Liu, Y. Li, Z. Liang, Z. Bao, Y. Cui, Surface fluorination of reactive battery anode materials for enhanced stability, J. Am. Chem. Soc. 139 (2017) 11550–11558.
[45] S.B. Son, L. Cao, T. Yoon, A. Cresce, S.E. Hafner, J. Liu, M. Groner, K. Xu, C. Ban, Interfacially induced cascading failure in graphite-silicon composite anodes, Adv. Sci. 6 (2019), 1801007.
[46] P. Parikh, M. Sina, A. Banerjee, X. Wang, M.S. D'Souza, J.-M. Doux, E.A. Wu, O. Y. Trieu, Y. Gong, Q. Zhou, K. Snyder, Y.S. Meng, Role of polyacrylic acid (PAA) binder on the solid electrolyte interphase in silicon anodes, Chem. Mater. 31 (2019) 2535–2544.
[47] D. Aurbach, I. Weissman, A. Schechter, X-ray photoelectron spectroscopy studies of lithium surfaces prepared in several important electrolyte solutions. A comparison with previous studies by Fourier transform infrared spectroscopy, Langmuir 12 (1996) 3993.
[48] Tf Yi, L. Shi, X. Han, F. Wang, Y. Zhu, Y. Xie, Approaching high-performance lithium storage materials by constructing hierarchical $CoNiO_2$@CeO_2 nanosheets, Energy Environ. Mater. 4 (2020) 586–595.
[49] T.-T. Wei, P. Peng, Y.-R. Ji, Y.-R. Zhu, T.-F. Yi, Y. Xie, Rational construction and decoration of Li5Cr7Ti6O25@C nanofibers as stable lithium storage materials, J. Energy Chem. 71 (2022) 400–410.
[50] A.M. Andersson, K. Edström, Chemical composition and morphology of the elevated temperature SEI on graphite, J. Electrochem. Soc. 148 (2001).
[51] W. Huang, J. Wang, M.R. Braun, Z. Zhang, Y. Li, D.T. Boyle, P.C. McIntyre, Y. Cui, Dynamic structure and chemistry of the silicon solid-electrolyte interphase visualized by cryogenic electron microscopy, Matter 1 (2019) 1232–1245.
[52] T.-F. Yi, L.-Y. Qiu, J. Mei, S.-Y. Qi, P. Cui, S. Luo, Y.-R. Zhu, Y. Xie, Y.-B. He, Porous spherical NiO@NiMoO4@PPy nanoarchitectures as advanced electrochemical pseudocapacitor materials, Sci. Bull. 65 (2020) 546–556.
[53] T. Mu, Y. Zhao, C. Zhao, N.G. Holmes, S. Lou, J. Li, W. Li, M. He, Y. Sun, C. Du, R. Li, J. Wang, G. Yin, X. Sun, Stable silicon anodes by molecular layer deposited artificial zincone coatings, Adv. Funct. Mater. 31 (2021), 2010526.
[54] N. Leventis, C. Chidambareswarapattar, A. Bang, C. Sotiriou-Leventis, Cocoon-in-web-like superhydrophobic aerogels from hydrophilic polyurea and use in environmental remediation, ACS Appl. Mater. Interfaces 6 (2014) 6872–6882.
[55] P. Li, J.Y. Hwang, Y.K. Sun, Nano/microstructured silicon-graphite composite anode for high-energy-density Li-ion battery, ACS Nano 13 (2019) 2624–2633.

Tiansheng Mu is currently a postdoctoral researcher at Harbin Institute of Technology (HIT), China. He received his Ph.D. degree at HIT in 2021. Meanwhile, he studied as a CSC visiting Ph.D. student under the supervision of Prof. Xueliang Sun for two years from 2019 to 2021 at the University of Western Ontario, Canada. Currently, his research interests mainly focus on the design and construction of anode materials for lithium-ion batteries.

Yipeng Sun is currently a Ph.D. candidate in Prof. Xueliang (Andy) Sun's Group at the University of Western Ontario, Canada. He is also under the co-supervision of Prof. Tsun-Kong (T.K.) Sham at the University of Western Ontario. He received his B.Eng. degree in Polymer Science and Engineering from Sichuan University (Chengdu, China) in 2016. His research interests focus on the interface modification of electrode materials for lithium-ion batteries.

Dr. Changhong Wang is currently a research scientist in GLABAT Solid-State Inc. Canada. He obtained his M.S. degree in Materials Engineering in 2014 from University of Science and Technology of China (USTC) and received his Ph.D. degree in Mechanical and Materials Engineering from the University of Western Ontario (UWO), Canada. He also served as a research assistant in Singapore University of Technology and Design (SUTD) from 2014 to 2016. Currently, his research interests include solid-state sulfide electrolytes, all-solid-state batteries, and bio-inspired artificial synapses.

Dr. Yang Zhao is an Assistant Professor in the Department of Mechanical and Materials Engineering at the University of Western Ontario, Canada. Dr. Zhao received his B.S. and M.S. degrees from Northwestern Polytechnical University (Xi'an, China) in 2011 and 2014, respectively. He obtained his Ph.D. degree under the supervisor of Prof. Xueliang (Andy) Sun from the University of Western Ontario in 2018. Then, he had his postdoc training at Western and the Advanced Light Source of Lawrence Berkeley National Laboratory in 2019–2020. His research interests focus on advanced materials and interfaces for energy storage applications, and synchrotron-based X-ray techniques.

Kieran Doyle-Davis received his Honors B.Sc. in Physics from McMaster University in 2018, with research focus on process optimization for lithium ion battery fabrication, and thin polymer films. Kieran is currently an MESc candidate at the University of Western Ontario under the supervision of Prof. Xueliang Sun. His current research interests include the development of next generation surface modified 3-D current collectors for both solution and solid-state lithium ion batteries.

Jianneng Liang received his B.Sc. in Metallurgical Engineering from the Central South University in 2015. He now is currently a Ph.D. candidate in Prof. Xueliang (Andy) Sun's Nanomaterials and Energy Group at the University of Western Ontario, Canada. His research focus includes the interface designs for lithium battery, solid-state electrolyte synthesis, and high energy density cathode materials.

Dr. Xulei Sui currently is a lecturer at School of Chemistry and Chemical Engineering in Harbin Institute of Technology (HIT), China. He received his Ph.D. degree from HIT in 2015. Now he is also a postdoctoral fellow assisting Prof. Xue-Liang (Andy) Sun at University of Western Ontario, Canada and Prof. Zhen-Bo Wang at HIT. His current research interests are focused on the design and synthesis of advanced nano-materials for electrocatalysis in fuel cells.

Ruying Li is a research engineer at Prof. Xueliang (Andy) Sun's Nanomaterial and Energy Group at the University of Western Ontario, Canada. She received her Master degree in Material Chemistry under the supervision of Prof. George Thompson in 1999 at University of Manchester, UK, followed by work as a research assistant under the direction of Prof. Keith Mitchell at the University of British Columbia and under the direction of Prof. Jean-Pol Dodelet at I'Institut national de la recherché scientifique, Canada. Her current research interests are associated with synthesis of nanomaterials for electrochemical energy storage and conversion.

Chunyu Du is a Professor in School of Chemistry and Chemical Engineering at Harbin Institute of Technology (HIT), China. He received his B. E., M. E. and Ph.D. degree at HIT in 1998, 2000 and 2004, respectively. He was a postdoctoral fellow at Hong Kong University of Science and Technology in 2006–2007. His current research interests are associated with high-performance ternary (NCA, NCM), Li-rich cathode materials for LIBs and advanced electrocatalysis in PEMFCs.

Pengjian Zuo is currently a Professor in School of Chemistry and Chemical Engineering at Harbin Institute of Technology (HIT). He received the B.E. and Ph.D. degree in Chemical Engineering and Technology at HIT in 2002 and 2007, respectively. He had been a visiting scholar at Pacific Northwest National Laboratory and Brookhaven National Laboratory in 2012–2013 and 2017 respectively. His research interests focus on energy storage materials and high-performance energy storage/conversion systems including lithium/sodium ion batteries, lithium/magnesium sulfur batteries and lithium metal batteries.

Geping Yin is currently a Full Professor in School of Chemistry and Chemical Engineering at the Harbin Institute of Technology (HIT), China. She got her bachelor degree in Electrochemical Engineering at HIT in 1982, and then received her Ph. D. degree in 2000. She got to Tokyo Institute of Technology and Yokohama National University as a senior visiting scholar in 1985 and 2008, respectively. She has continuously entered the list of the Elsevier Most Cited Chinese Researchers since 2015. Her current research interests focus on electrocatalysis for PEMFC, Aluminum-air batteries, electrode materials and battery management for lithium-ion batteries.

Prof. Xueliang Sun is a Canada Research Chair in Development of Nanomaterials for Clean Energy, Fellow of the Royal Society of Canada and Canadian Academy of Engineering and Full Professor at the University of Western Ontario, Canada. Dr. Sun received his Ph.D. in materials chemistry in 1999 from the University of Manchester, UK, which he followed up by working as a postdoctoral fellow at the University of British Columbia, Canada. His current research interests are focused on advanced materials for electrochemical energy storage and conversion, including electrocatalysis in fuel cells and electrodes in lithium-based batteries, metal-air batteries and solid-state batteries.